Geomechanics and Engineering, *Vol. 17, No. 4 (2019) 375-383*
DOI: https://doi.org/10.12989/gae.2019.17.4.375

Microseismic monitoring and its precursory parameter of hard roof collapse in longwall faces: A case study

Jun Wang[a], Jianguo Ning*, Pengqi Qiu**, Shang Yang[b] and Hefu Shang[c]

State Key Laboratory of Mining Disaster Prevention and Control Co-founded by Shandong Province and the Ministry of Science and Technology, Shandong University of Science and Technology,579 Qianwangang Road, Qingdao, China

(Received August 18, 2018, Revised February 11, 2019, Accepted March 4, 2019)

Abstract. In underground retreating longwall coal mining, hard roof collapse is one of the most challenging safety problems for mined-out areas. Identifying precursors for hard roof collapse is of great importance for the development of warning systems related to collapse geohazards and ground control. In this case study, the Xinhe mine was chosen because it is a standard mine and the minable coal seam usually lies beneath hard strata. Real-time monitoring of hard roof collapse was performed in longwall face 5301 of the Xinhe mine using support resistance and microseismic (MS) monitoring; five hard roof collapse cases were identified. To reveal the characteristics of MS activity during hard roof collapse development and to identify its precursors, the change in MS parameters, such as MS event rate, energy release, bursting strain energy, b value and the relationships with hard roof collapse, were studied. This research indicates that some MS parameters showed irregularity before hard roof collapse. For the Xinhe coalmine, a substantial decrease in b value and a rapid increase in MS event rate were reliable hard roof collapse precursors. It is suggested that the b value has the highest predictive sensitivity, and the MS event rate has the second highest.

Keywords: hard roof collapse; microseismic monitoring; precursory parameter; support pressure

1. Introduction

Hard roof collapse has always been a major concern in underground coalmines (Ning *et al*. 2017a, Mohammadi *et al*. 2018, Liu *et al*. 2018). Hard roof collapse could cause fatalities, injuries, equipment damage and significant economic losses (Hosseini 2017, Jiang *et al* 2019). A proper understanding of hard strata failure is essential in order to provide timely warnings for geohazards related to roof collapse and to take remedial measures (Ning *et al*. 2018, Wang *et al*. 2018). Recently, MS monitoring has been developed based on the understanding of the mechanisms and geotechnical precursors of hard strata collapse (Mondal *et al*. 2017). If some common MS precursors for hard strata collapse are identified, remedial measures could be taken in a timely manner to prevent adverse effects.

Numerous studies have been performed to investigate the mechanisms of roof collapse in underground coalmines, and they have suggested various geotechnical precursors of roof collapse related to underground mining activities, including displacement, stress, and acoustic emission (Gholizadeh *et al*. 2015, Jiang *et al*. 2017, Zhang *et al.* 2018, Liu *et al*. 2018). Szwedzicki (2001) stated that displacement monitoring, although it provides valuable information on structural damages of rock masses, appears to have limited value in providing the time of the collapse. Iannacchione *et al.* (2004) performed a field study in an underground stone mine to investigate roof falls and roof caving events and suggested that, in the roof fall area, MS activity increased significantly before roof displacement. Shen *et al.* (2008) applied an "integrated roof monitoring system" to investigate gateroad roof fall in underground mines and found that seismicity and stress changes can reliably indicate caving events. Gao *et al.* (2014) and Tien *et al.* (2018) performed a numerical study to simulate roof shear failure using the distinct element method and found similar geotechnical precursors of roof collapse. These studies indicated that it is difficult to evaluate precursory signs with traditional displacement and stress measurements because deformation prior to onset may be very small during brittle failure.

It is well recognized that rock fracture can be identified via MS activity. In recent years, MS systems have been used in underground excavations to gain a better understanding of the failure of surrounding rock. MS parameters, such as the energy index, Schmidt number and b value, have precursory characteristics before rock mass failure, and the Schmidt number has the highest predictive sensitivity (Mahdevari *et al.* 2016, Leake *et al.* 2017, Guo *et al.* 2018, Ghosh *et al.* 2018). Zhang *et al.* (2015) investigated the microseismicity associated with crown pillar failure in the Shirengou iron mine and proposed that, before failure occurred, the b value decreased rapidly and

*Corresponding author, Professor
E-mail: njglxh@126.com
**Corresponding author, Ph.D. Student
E-mail: qiupengqi@163.com
[a]Ph.D.
E-mail: wangjunsdkjd@126.com
[b]Student
E-mail: 879588836@qq.com
[c]Student
E-mail: shanghefu@126.com

ISSN: 2005-307X (Print), 2092-6219 (Online)

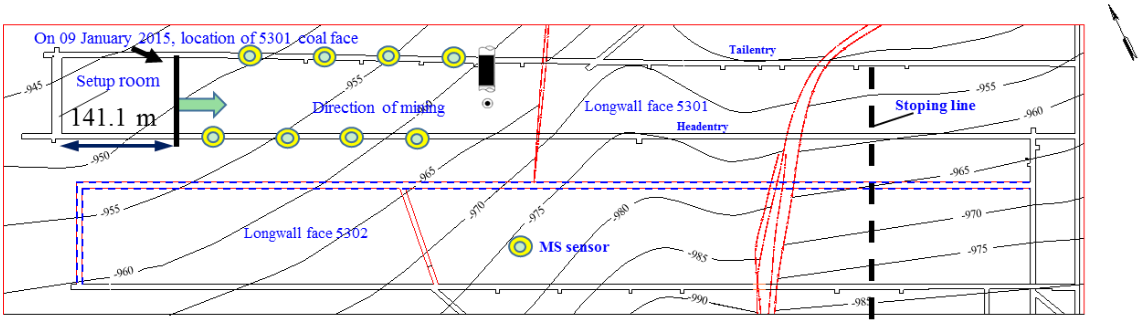

Fig. 1 Plan view of the local panel layout

MS apparent stress increased. Zhang *et al.* (2016) performed a field MS monitoring investigation in an underground phosphate mine to study the seismicity associated with roof caving events and found similar MS precursors of roof collapse. Dai *et al.* (2016) suggested that an abrupt increase in MS events accompanied by a sharp increase in apparent stress and a steady increase in cumulative volume can be used to forecast surrounding rock mass failure of underground powerhouse caverns. These studies provide meaningful achievements toward identifying MS precursors for roof failure; however, they all focus on small-scale roof failure in underground excavations and intersections. Currently, MS monitoring is being used for applications in some coalmines in China. Lu *et al.* (2016) investigated the relationships among hard and thick igneous strata separation, fracturing and MS intensity; they found that the energy ratio of MS events in low-frequency bands represent an effective index for predicting the intensity of roof fracture. Ning *et al.* (2017b) performed a field MS monitoring study in underground coalmines to investigate the progressive fracture failure procedure of double-layered hard and thick roofs. These studies indicated that MS source location, MS signal frequency, and the energy calculation with regard to common roof fracturing could be used to investigate the mining-induced response of hard strata (i.e., separation, fracture and collapse). These studies focused on the investigation of progressive movement and rock strata fracture based on the spatiotemporal distribution of MS events; however, to date, the identification of common MS precursors for hard strata collapse is still unresolved and the accuracy of prediction results cannot be easily evaluated.

To help understand the mechanisms associated with this problem, this paper presents a case study on the MS monitoring system in the Xinhe coalmine in China, where mineable coal seams are typically covered by hard strata. Through real-time MS monitoring, the relationships between hard roof collapse and the characteristics of MS activity are studied, and the precursory MS characteristics for hard roof collapse were identified.

2. Case study

2.1 Geological and mining conditions of the Xinhe mine

The site for the field test was located in the Xinhe coalmine, Shandong Province, China. Longwall face 5301 (LW 5301), as shown in Fig. 1, was chosen for this study. LW 5301 used the fully mechanized full-seam top-coal cave-mining method and extracted coal seam No.3. Coal seam No.3 is approximately 10.2 m thick on average and dipped 2°-6° with an average of 3°. The mining height of LW 5301 was 3.9 m and the top coal caving height was 11.4 m. Therefore, the ratio of the mining height to the top coal caving height was 1:2.9. The average daily face advance was 3.2 m. In Fig. 1, LW 5301 was 65 m wide by 844 m long. Both the northeast and northwest sides were unmined solid coal, and southwest side will arrange longwall face 5302.

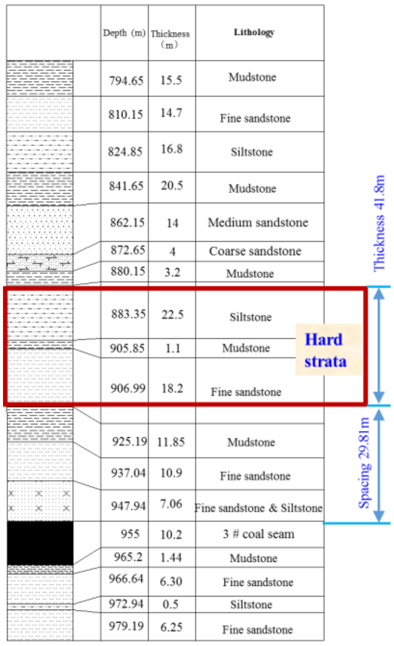

Fig. 2 Typical geological column

Fig. 2 presents a generalized stratigraphic column of the study site, which is constructed base on core logging. The roof stratum of LW 5301 is mainly composed of mudstone, fine sandstone, and siltstone. The immediate roof was sandstone, siltstone, fine sandstone and mudstone with an average thickness of 29.8 m. The main roof was fine sandstone and siltstone with an average thickness of 41.8 m. Sandstone and siltstone have a uniaxial compressive strength of 86.5-173.7 MPa (with a mean of 130.1 MPa) and 77.6-124.8 MPa (with a mean of 101.2 MPa), respectively. The main roof was hard and strong.

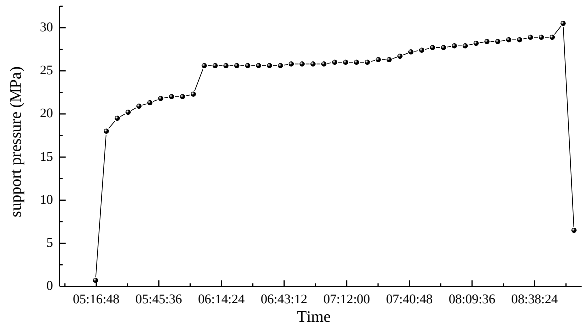

Fig. 3 Monitored support resistance variation in a mining cycle

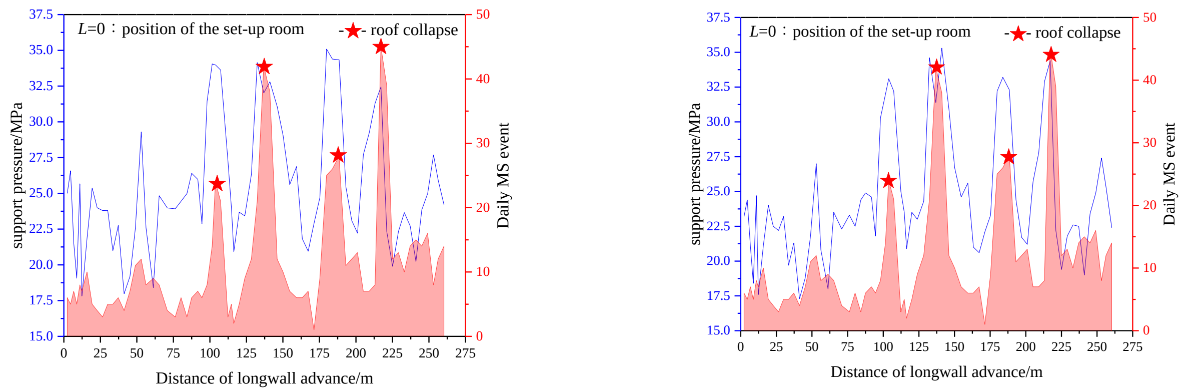

(a) NO. 56 support (b) NO. 80 support

Fig. 4 Changes in the maximum resistance of the support as the face advances

2.2 MS monitoring system and sensor arrangement

A 16-channel ARAMIS M/E MS system developed by the Poland Institute of Innovative Techniques was installed at the Xinhe coalmine on October 13, 2015. This monitoring system consisted of a central computer, a real-time monitoring recorder server, sensors and a digital transmission system. The monitoring frequency range of a single sensor was 0-150 Hz, and it had a sensibility of 110 mV/s ± 10%, a sampling rate of 500 Hz, and a 12-bit A/D converter. The system can automatically identify mining-induced MS signals. Meanwhile, the quantitatively calculated MS parameters, such as occurrence time, released energy (≥ 100 J) and event location, can be determined using the Powell location algorithm. To determine the spatial location of seismic sources, the constant velocity model (VP = 4000 m/s for geophones #1–6; VP = 3000 m/s for geophones #7–10; and VP = 2800 m/s for geophone #16) was used.

A total of fourteen sensors was installed in the underground mine, and their arrangement satisfies the D-value optimization criteria. LW 5301 was surrounded by eight sensors. To understand the space positioning accuracy of the MS system, field blasting tests were performed at known locations. The known coordinates were compared with the coordinates of the MS system analysis, which indicated that the source location accuracy can satisfy the engineering requirements. For MS signal processing, the blasting signal, vibrational signal of the machine and other unwanted signals were manually filtered out. Meanwhile, rock fracture MS events were identified.

2.3 Description of hard roof collapse

In past investigations, it has been found that roof pressure (i.e., support pressure) is at its maximum when the hard strata near the immediate roof breaks and collapses into the caved zone (Peng 2013, Dyke *et al.* 2018). In this case, to indirectly capture hard roof collapse, the support pressure/resistance is generally monitored as the longwall face advances. Fig. 3 shows the monitored support resistance in the field in a mining cycle.

Variations in the pattern of the support resistance have been encountered in underground coal mining depending upon support operations, geological conditions, mining methods, etc. In general, the pattern of support resistance can be classified into four types during one pass of the longwall shearer: initial setting period, rapid increasing resistance period, cutting influenced period, and rapid decreasing resistance period (Peng 1987). As shown in Fig. 3, the monitored support resistance also showed four patterns in a mining cycle. This is in agreement with the field results in a previous study by Peng (1987). In longwall mining, the maximum resistance of the support in each mining cycle was generally obtained and used to as an indicator to evaluate roof activities (Paul 2016, Wang *et al.* 2017). Fig. 4 shows the typical variations of the maximum resistance of the support (MRSS) with face advancement.

As shown in Fig. 4, MRSS exhibited an apparent correlation with longwall face advancement, which reflects the various degrees of roof activity. Using NO. 56 support as an example, it can be seen that the MRSS showed no considerable increase after the coalface advanced

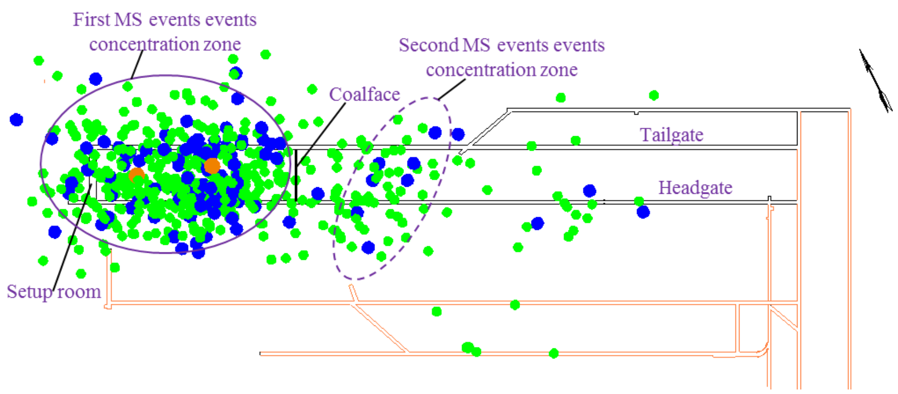

(a) Planar distribution

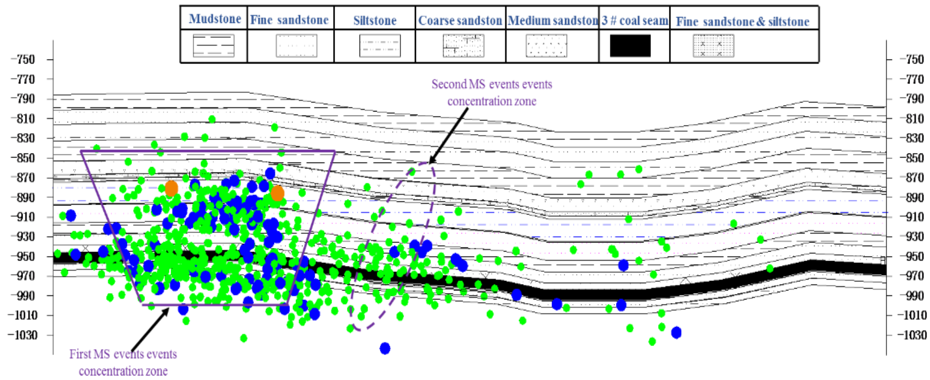

(b) Vertical distribution

Fig. 5 (a) Planar and (b) vertical distributions of MS events during the mining of LW 5301 (from 28th November, 2015 to 28th January, 2016). Note: color denotes energy release (green: 0–3.5×103J; blue: 3×103–104J; orange > 104J) (Ning *et al.* 2017b)

approximately 30 m, indicating that local fall of the roof had not occurred. A slight increase in MRSS was observed during roof caving after the face advanced 52.9 m. Subsequently, MRSS increases to its peak (approximately 35 MPa) at 103.9-107.35 m face advancement, indicating that the first significant collapse of the main roof occurred. The first periodic collapse of the main roof is exhibited at 103.9-107.35 m face advancement with 35-40 MPa load on the support. The subsequent periodic collapses of the main roof occurred after coalface advancements of 136.9–141.1 m, 183.9-188.5 m, and 213.1-217.1 m. In other observations (NO. 80 support), the MRSS curve varied up and down, which is related to the main roof collapsing.

Field investigation showed that some of the supports reached the yield pressure during the main roof collapse (Singh 2015, Yin *et al.* 2018). The yield pressure was maintained from three to seven, and thereafter, the support pressure began to return to normal. In addition, the spalling of the face increased during the main roof collapse due to the increase in ground pressure. These findings substantiate the previous finding that the failure of the hard roof, over large spans, causes roof pressure at the face, which results in the loading of the support and high abutment stress during roof collapses. Therefore, since the high support pressure appeared right after the occurrence of the main roof collapse, it could not be used to develop an early warning for hard roof collapse.

3. Characteristics of MS activity in longwall mining

Using the ARAMISM/E monitoring system, mining-induced MS events of LW 5301 in the Xinhe coalmine were obtained. Then, the relationships between mining-induced rock failure and the changes in MS parameters were studied.

3.1 MS activity characteristics

3.1.1 Spatial distribution of MS events

Fig. 5 showed the spatial distribution of MS events from 28th November, 2015, to 28th January, 2016. During this period, 729 rock failure MS events were obtained.

As shown in Fig. 5(a), the MS events mainly concentrated in two zones. The first MS event concentration zone is close to LW 5301 and the two sides of the 5301 working face roadway, which is closely related to coal mining the working face. Thus, the first MS event concentration zone is mainly impacted by mining the working face. In general, the envelope of MS events induced by coal mining has an elliptical shape (Fig. 5(a)), which is in similar with the so-called “O” ring proposed by Guo *et al.* (2012) and Yin *et al.* (2018). Meanwhile, this envelope displays an inverted trapezoid shape in the side view (Fig. 5(b)), which is agreement with the result of Islam *et al.* (2009).

The second MS event concentration zone was in front of the coalface of LW 5301; the distance between them was approximately 80–120 m, where there is a fault according to the in situ geological survey, and the planar view has a skew distribution. Hence, the occurrence of this MS event concentration zone was mainly influenced by the geological structure, possibly indicating the reactivation of faults by the interaction of existing tectonic stress and mining-induced stress.

3.1.2 MS event rate characteristics

MS event is the one of MS basic parameters for field monitoring, and it is the simplest indicator of rock fracturing. Fig. 6 presents the variations of the monitored MS event rate from 28th November, 2016 to 28th January, 2017. It is should be noted that the MS event rate is the total number of MS event generated daily. During this period, LW 5301 had advanced 221.1 m from the initial location.

The plot of MS event rate with face advancement showed that the daily MS event rate was very low (with an average of 6.5 per day) before the 52.9-m advance. Immediately after the longwall face advanced 52.9 m, the MS event rate slightly increased due to the roof caving. However, the daily MS event rate increase rapidly at 103.9-107.35 m face advancement. At this time, field support resistance was rising and intense ground pressure behavior appeared, which indicated the main roof break and collapse for the first time; the first collapsing interval (i.e., the first weighting interval) was approximately 103.9-107.35 m, which was almost consistent with the results obtained using the method of monitoring support resistance (introduced in Section 2.3). After the first collapse of the hard main roof, the MS event rate decreased to a low level. Subsequent periodic increases in the MS event rate were observed after the face advanced 136.9-141.1 m, 183.9-188.5 m, and 213.1-217.1 m, which exhibited an apparent correlation with the periodic collapse of hard main roof. Additionally, during a non-periodic collapsing period, MS activity entered a "quiet period," indicating that the MS event rate was low. As the hard main roof broke and collapsed, the incidence of MS activities increased dramatically, i.e., the MS active period is approximately 2 days. MS activities appeared in the form of foreshocks, main shock, and aftershocks. It can be seen that the collapse of the hard main roof coincided with the increasing MS event rate, which agrees with the results of Iannacchione *et al*. (2005) and Li *et al*. (2016).

According to the analyses above, it can be found that the main shock, i.e., the increase in MS event rate, represents the collapse of the hard main roof, and the MS quiet period represents the instability of the hard main roof prior to collapse. Hence, the increase in MS event rate might be viewed as a precursor for hard roof collapse.

3.2 Energy release characteristics

The MS release energy (RE) is another basic parameter that can be used to describe microseismicity and interpret the state of fracture development in the rock mass. Fig. 7 shows the changes of daily MS total energy.

The plot of daily MS total energy against face advancement shows that the daily MS total energy has a periodic change phenomenon. It is interesting to see that, during the period of hard main roof collapse, the daily MS energy increased sharply, and then decreased to low level; there is also a considerable increase in the daily MS energy at other times. For example, with a distance advancement of 103.9-107.35 m, 136.9-141.1 m, 183.9-188.5 m, and 213.1-217.1 m, the first main roof collapse was observed, and simultaneously, MS energy release suddenly reached its maximum. However, there is an unusual increase in the daily MS energy at 116.35-120.1 m and 241.1-249.1 m face advancement when the hard main roof did not fail and collapse. At this time, the instability of the surrounding rock or the large deformation of the roadway was observed in the field. It can be seen that the two high MS energy releases above had no obvious relationship with hard main roof collapse, but the mining-induced local failure of surrounding rock did. This because that the daily MS event rate was low in that day; thus, one or several high-energy MS events that may be generated by the mining-induced local failure of surrounding rock could improve the quantity of the total daily MS energy.

According to the analyses above, the bigger the MS energy release, the higher the deformation and failure intensity of the rock and coal materials. However, a high MS energy release not only depends on the roof movement of the longwall face but also the mine pressure induced by the surrounding rock failure induced by the change in mine pressure. Hence, a high MS energy release might not be

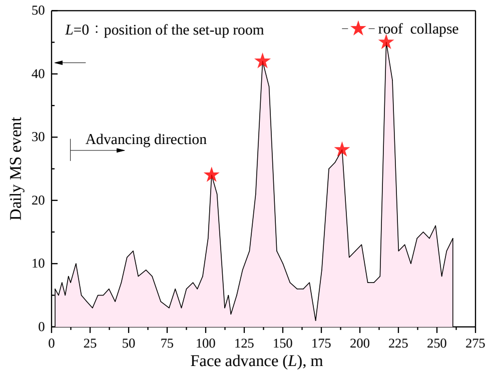

Fig. 6 Change in MS activity with advancement distance during the selected period

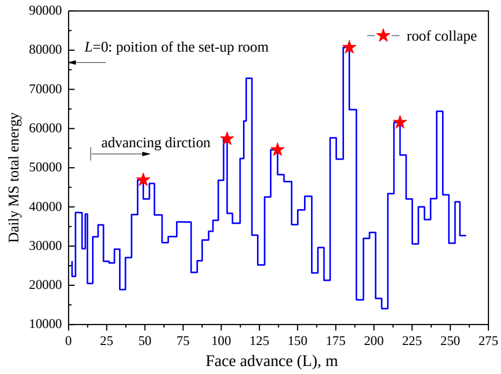

Fig. 7 Change of daily MS total energy with advancement distance during the selected period

Table 1 Relationship between BSE index and rock burst risk (Cao *et al*. 2018)

Risk index	Rock burst risk degree	BSE index $W_{\varepsilon t}$
0	None	<
1	Weak	0.25 to 0.5
2	Moderate	0.5 to 0.75
3	Strong	> 0.75

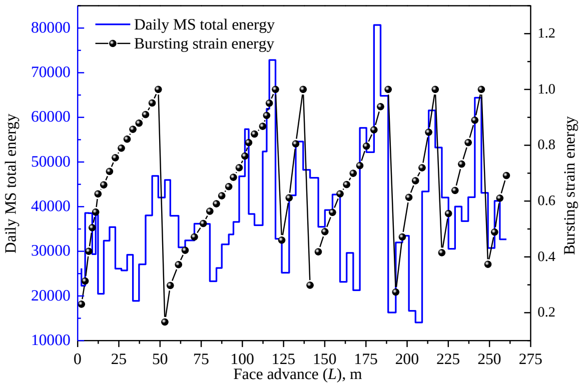

Fig. 8 Change in BSE with advancement distance during the selected period

regarded as an effective precursory sign for the collapse of the hard main roof.

3.3 Bursting strain energy characteristics

It has been found that roof collapse occurs due to the formation of fractures and causes a reduction in the stress or strain rebound (Huang *et al*. 2018, Mohammadi *et al*. 2018). To characterize a particular fracture scale, bursting strain energy (BSE) Wεt was established (Cao *et al*. 2018). BSE is an important parameter used to predict and warn against rock-burst hazards induced by hard roof fall in China. Table 1 lists the grade division for rock burst warnings. $W_{\varepsilon t}$ is developed as follows

$$W_{\varepsilon t}=\frac{\varepsilon_E-\varepsilon_{E0}}{\varepsilon_{El}-\varepsilon_{E0}},\ \varepsilon_E=\sum_{i=1}^{n}\sqrt{E_i} \tag{1}$$

where εE is a specific equivalent strain, Ei is the released energy of the ith MS event after the last macro-fracture, εE0 is the initial equivalent strain, and its default setting is 0, and εEl is the critical equivalent strain. For interpretation of the references to the computational method of the above parameters, refer to the web version of reference (Cao *et al*. 2018).

Fig. 8 presents typical curves for BSE and the total daily MS energy for MS events with longwall face advancement. As shown in Fig. 8, BSE almost corresponds with the occurrence of a high-energy release. Before the appearance of a high-energy MS release, Wεt indicated a strong rock burst risk. In particular, Wεt remained at a strong rock burst risk level since the coalface advanced approximately 45.25 m, 114.75 m, 132.4 m, 179.9 m, 209.1 m, and 237.1 m, and then reached the critical feature value after 2–3 days until the occurrence of the high-energy release. Thereafter, BSE and MS RE decreased rapidly. Interestingly, prior to the occurrence of hard main roof collapse, there were no significant changes in BSE Wεt. For example, prior to the occurrence of the first main roof collapse, Wεt was approximately 75%. However, when the periodic collapse of the main roof occurred (the coalface advanced approximately 103.9-107.35 m, 136.9-141.1 m, 183.9-188.5 m, and 213.1-217.1 m), BSE almost reached the critical feature value of 1. According to the calculation method, BSE had an obvious positive correlation with MS energy release. Thus, critical feature values were observed in space domain BSE curve when the coalface advanced approximately 120.1 m and 245.1 m (the periodic collapse of the main roof did not occur).

According to the analyses above, it can be found that the bigger the MS energy release, the higher the deformation and failure intensity of rock and coal materials. However, the high-energy MS release depends not only on the roof movement of the longwall face but also the mine pressure induced by the surrounding rock failure induced by the change in mine pressure. Hence, high-energy MS release might not be able to be used as an effective precursory warning for hard main roof collapse.

3.4 b value characteristics

In a previous study, it has been found that mining-induced MS events followed some of the same rules as the magnitude-frequency relationship in natural earthquake seismology, for which Gutenberg and Richter proposed the empirical formula (Gutenberg and Richter 1944).

$$\lg N=a-bM \tag{2}$$

where M is the magnitude, N is the number of earthquakes with a magnitude equal or above M, and a and b are constants. The change in b is closely related to the fracture extension scale, and the declining trend of b implies crack growth and the increase of large cracks.

Utsu *et al*. (1995) suggested that, if the magnitude distribution obeys the G-R relation, the b value may be calculated by the maximum likelihood method, which delivers better results than the least squares method. Therefore, in this paper, the maximum likelihood method was used to calculate the b value

$$b=\frac{0.4343}{\overline{M}-M_0} \tag{3}$$

$$\overline{M}=\sum_{i=1}^{N}\frac{m_i}{N} \tag{4}$$

where $\overline{M}$ is the average of the MS energy in the statistical period, N is the total number of MS events, and M0 is the lower limit of the MS energy used for analysis. In this study, M0 = 0.2 was used because magnitude M - 5.5 means.

The changes in b value and energy release are shown in Fig. 9. We focus mainly on the variation in b value with

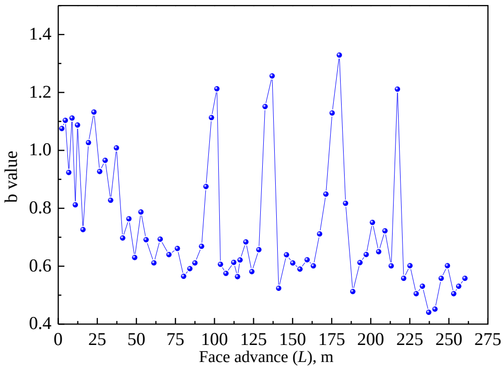

Fig. 9 Change in b value with advancement distance during the selected period

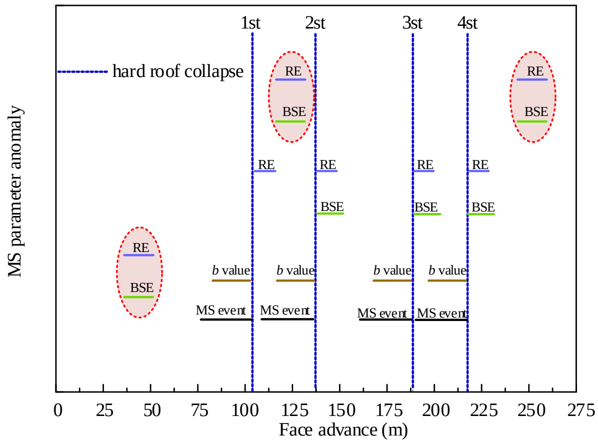

Fig. 10 MS parameter anomaly with advance distance

changes in longwall face advancement. Observations can be generalized as follows:

(1) At advancement distances of 91.75-103.55 m, 128.4-136.9 m, 167.3-179.9 m, and 209.1-213.1 m, b value increased rapidly, support pressure rose slightly and hard roof collapse did not occur. The results indicate that small-scale cracks also increased with ground pressure and low-magnitude events are more numerous than high-magnitude events. In other words, surrounding rock may be instable, leading to the generation of high-magnitude events.

(2) When the coalface advanced 103.9-107.35 m, 136.9-141.1 m, 183.9-188.5 m, and 213.1-217.1 m, b value declined rapidly, indicating that small-scale cracks in surrounding rock gradually propagated to produce larger cracks and rock failure. Energy release also increased rapidly and larger cracks were generated. At this time, the field support pressure increased sharply and the hard roof failed and collapsed.

(3) After hard roof collapse, b value stabilized, which means that crack extension is stable. When the b values are stable, the hard roof is relatively quiet. Field investigation has found that, at the advance distances of 0-91.75 m, 107.35-128.4 m, 141.1-167.3 m, and 188.5-209.1 m, the hard roof did not fail and collapse.

Based on this analysis, it can be found that, before hard roof collapse, b value first increases and then decreases. When b value declines rapidly, hard roof collapsing will follow. Therefore, these two stages of rapid decline in b value could be regarded as an effective precursory sign for hard roof collapse.

4. Discussion

Identifying MS precursory parameters for hard roof collapse is essential for mine design to be adjusted in a timely manner and remedial measures to be taken. The MS monitoring system provided us with a large amount of data, which has improved our understanding of hard roof behavior and failure processes. As seen from the above analysis, MS parameters performed uncharacteristically before or after hard roof collapse. MS event rate, RE, and BSE increased rapidly, and b value decreased sharply. MS parameter anomalies with distance advancement were plotted in Fig. 10. In Fig. 10, the blue dotted line represented the locations of hard roof collapse. The reddish ellipse meant that the hard roof did not collapse.

Table 2 Predictive periods divided by parameters

Roof strata state	MS parameter
immediate roof caving	MS event rate
hard roof collapsing	MS event rate, *b* value

As shown in Fig. 10, RE and BSE were abnormal when hard roof collapse was occurring or had occurred, but the b value and MS event rate were abnormal before the hard roof collapse occurred, which means that MS event rate and b value had precursory characteristics and forecasting significance for hard roof collapse. Other authors (Li *et al.* 2016, Hosseini 2017) found that MS parameters, such as MS event rate and b value, can be regarded as precursory signs to warn of rock mass failure, and their results are consistent with those in this study. RE and BSE can effectively represent the rock energy accumulation, damage, and release processes during longwall mining. Hard roof collapse, as a kind of ground pressure behavior, has a close relationship with energy release. The calculation accuracy of MS event energy release in the MS monitoring test depends on the wave velocities of roof strata. It should be noted that roof strata "anisotropic" material and wave velocities could vary, and so there existed a small error in the calculation of MS event energy release. Moreover, during the non-collapse period of the hard roof, some large surrounding rock failure also released energy. Hence, RE and BSE might be not regarded as an effective precursors to evaluate hard roof collapse events.

Kang *et al.* (2018) suggested that hard roof collapse was a result of micro-crack initiation and unstable propagation. In the case of progressive strata failure, the number of MS activities increases intensely due to the strata transition from a stable state to an unstable state. Field monitoring showed that the onset of changes in MS event rate and b value signaled the beginning of unstable conditions. Hence, MS event rate and b value can reliably warn of hard roof collapse events. The predictive periods estimated by MS event rate and b value are shown in Table 2. Concerning the predictive frequency, MS event rate was uncharacteristic five times, but b value was four times. MS event rate appeared anomalous immediately before roof caving and during hard roof collapse. Hence, b value has the highest predictive sensitivity. The sensitivity analysis is only for the results of MS monitoring in this paper.

The field experiments concentrated on hard roof collapse induced by longwall mining. Although it is expected that the identified MS precursors are common for all hard roof collapses in underground coalmines, they should be validated against various roof strata cave-in modes (Diederichs and Kaiser 1999) in simple geological conditions without large surrounding rock failure. This verification can be done via field experimentation in underground longwall coalmines. It is very difficult to conduct a single monitoring experiment in an operating mine to observe normal hard roof collapse because there are many types of geological anomalies and discontinuities in the targeted longwall face and the stratigraphic sequence above the coal seam varies between parts of the same panel. Different geological conditions or stratigraphic sequences will induce different roof strata cave-in types.

5. Conclusions

In this paper, real-time MS monitoring has been applied in the Xinhe coalmine, where the mineable coal seams are typically covered by hard and thick strata. The MS monitoring system provided us with a large amount of data on roof strata behavior, which improved our understanding of precursory parameters for hard roof collapse. The main conclusions are as follows:

From the change in support pressure, it can be seen that the first hard roof collapse occurred when longwall face 5301 advanced 103.9-107.35 m from the initial location. The periodic collapse of the hard roof occurred when the longwall face advanced 136.9-141.1 m, 183.9-188.5 m and 217.1-225.1m. The first weighting interval was approximately 103.9-107.35 m and the periodic weighting interval was approximately 33-42.8 m.

For the Xinhe coalmine, the change in the MS parameters, including MS event rate, energy release, bursting strain energy and b value, depends on the mine pressure change of the longwall face. Mine pressure, MS event rate, energy release, and bursting strain energy increased quickly, but b value suddenly and sharply decreased.

The characteristic analysis found that MS event rate, energy release, bursting strain energy and b value became anomalous before or after hard roof collapse. For the Xinhe coalmine, MS event rate and b value can be regard as precursory parameters for hard roof collapse; b value has the highest predictive sensitivity, and the predictive sensitivity of MS event rate was the second highest.

Acknowledgements

This study was supported by National Key R&D Program of China (2018YFC0604703), the National Natural Science Foundation of China (No. 51574154), the Shandong Province Science and Technology Development Plan, item (2014GSF120002), and Key R & D project of Shandong Province (2018GSF116003). Natural Science Foundation of Shandong Province (ZR2017BEE013, ZR2018QEE0020)

References

Cao, A.Y., Dou, L.M., Wang, C.B., Yao, X.X., Dong, J.Y. and Gu, Y. (2016), "Microseismic precursory characteristics of rock burst hazard in mining areas near a large residual coal pillar: A case study from Xuzhuang coal mine, Xuzhou, China", *Rock Mech. Rock Eng.*, **49**(11), 1-16.

Dai, F., Li, B., Xu, N. Fan, Y.L. and Zhang, C.Q. (2016), "Deformation forecasting and stability analysis of large-scale underground powerhouse caverns from microseismic monitoring", *Int. J. Rock Mech. Min. Sci.*, **86**, 269-281.

Diederichs, M.S. and Kaiser, P.K. (1999), "Stability of large excavations in laminated hard rock masses: the voussoir analogue revisited", *Int. J. Rock Mech. Min. Sci.*, **36**(1), 97-117.

Dyke, M.A.V, Su, W.H. and Wickline, J. (2018), "Evaluation of seismic potential in a longwall mine with massive sandstone roof under deep overburden", *Int. J. Min. Technol.*, **28**(1), 115-119.

Gao, F., Stead, D. and Kang, H. (2014), "Simulation of roof shear failure in coal mine roadways using an innovative UDEC Trigon approach", *Comput. Geotech.*, **61**(3), 33-41.

Gholizadeh, S., Leman, Z. and Baharudin, B.T.H.T. (2015), "A review of the application of acoustic emission technique in engineering", *Struct. Eng. Mech.*, **54**(6), 1075-1095.

Ghosh, G.K. and Sivakumar, C. (2018), "Application of underground microseismic monitoring for ground failure and secure longwall coal mining operation: A case study in an Indian mine", *J. Appl. Geophys.*, **150**, 21-39.

Guo, H., Yuan, L., Shen, B.T., Qu, Q.D. and Xue, J.H. (2012), "Mining-induced strata stress changes, fractures and gas flow dynamics in multi-seam longwall mining", *Int. J. Min. Technol.*, **54**, 129-139.

Guo, W.Y., Tan, Y.L., Yu, F.H., Zhao, T.B., Hu, S.C., Huang, D.M. and Qin, Z.W. (2018), "Mechanical behavior of rock-coal-rock specimens with different coal thicknesses", *Geomech. Eng.*, **15**(4), 1017-1027.

Gutenberg, B. and Richter, C.F., (1944), "Frequency of earthquakes in California", *B. Seismol. Soc. Am.*, **34**(4), 185-188.

Hosseini, N. (2017), "Evaluation of the rockburst potential in longwall coal mining using passive seismic velocity tomography and image subtraction technique", *J. Seismol.*, **21**(1), 1-10.

Huang, W.P., Li, C., Zhang, L.W., Yuan, Q., Zheng, Y.S. and Liu, Y. (2018), "In situ identification of water-permeable fractured zone in overlying composite strata", *Int. J. Rock Mech. Min. Sci.*, **105**, 85-97.

Iannacchione, A.T, Esterhuizen, G.S, Swansonm P.L., Swanson P.L. and Chapman M.C. (2005) "Characteristics of mining-induced seismicity associated with roof falls and roof caving events", *Proceedings of the 40th US Rock Mechanics Symposium*, Anchorage, Alaska, U.S.A., January

Islam, M.R., Hayashi, D. and Kamruzzaman, A.B.M. (2009), "Finite element modeling of stress distributions and problems for multi-slice longwall mining in Bangladesh, with special reference to the Barapukuria coal mine", *Int. J. Coal. Geol.*, **78**(2), 91-109.

Jiang, L., Zhang, P., Chen, L., Hao, Z., Sainoki, A., Mitri, H.S. and Wang, Q.B. (2017), "Numerical approach for goaf-side entry layout and yield pillar design in fractured ground conditions", *Rock. Mech. Rock. Eng.*, **345**(10), 690-705

Jiang, L.S, Kong, P., Shu, J.M. and Fan, K.G. (2019), "Numerical analysis of support designs based on a case study of a longwall entry", *Rock Mech*. *Rock Eng*., 1-12.

Kang, H.P., Lou, J.F., Gao, F.Q., Yang, J.H. and Li, J.Z. (2018), "A physical and numerical investigation of sudden massive roof collapse during longwall coal retreat mining", *Int*. *J*. *Coal Geol*., **188**, 25-36.

Leake, M.R., Conrad, W.J., Westman, E.C., Afrou, S.G. and Molka, R.J. (2017), "Microseismic monitoring and analysis of induced seismicity source mechanisms in a retreating room and pillar coal mine in the Eastern United States", *Undergr*. *Sp*., **2**(2), 115-124.

Li, Y., Yang, T.H., Liu, H.L. Wang, H., Hou, X.G., Zhang, P.H. and Wang, P.T. (2016), "Real-time microseismic monitoring and its characteristic analysis in working face with high-intensity mining", *J*. *Appl*. *Geophys*., **132**, 152-163.

Liu, X.S., Tan, Y.L., Ning, J.G., Lu, Y.W. and Gu, Q.H. (2018), "Mechanical properties and damage constitutive model of coal in coal-rock combined body", *Int*. *J*. *Rock Mech*. *Min*. *Sci*., **110**, 140-150.

Lu, C.P., Liu, Y., Wang, H.Y. and Liu, P.F. (2016), "Microseismic signals of double-layer hard and thick igneous strata separation and fracturing", *Int*. *J*. *Coal Geol*., **160**, 28-41.

Mahdevari, S., Shahriar, K., Sharifzadeh, M. and Tannant, D.D. (2016), "Assessment of failure mechanisms in deep longwall faces based on mining-induced seismicity", *Arab*. *J*. *Geosci*., **9**(18), 709.

Mohammadi S., Ataei M. and Kakaie R. (2018), "Assessment of the importance of parameters affecting roof strata cavability in mechanized longwall mining", *Geotech*. *Geol*. *Eng*., **36**(4), 2667-2682.

Mondal, D., Roy, P.N.S. and Behera, P.K. (2017), "Use of correlation fractal dimension signatures for understanding the overlying strata dynamics in longwall coal mines" *Int*. *J*. *Rock Mech*. *Min*. *Sci*., **91,** 210-221.

Ning, J.G., Wang, J., Jiang, J.Q., Hu, S.C., Jiang, L.S. and Liu, X.S. (2018), "Estimation of crack initiation and propagation thresholds of confined brittle coal specimens based on energy dissipation theory", *Rock Mech*. *Rock Eng*., **51**(1), 119-134.

Ning, J.G., Wang, J., Jiang, L.S., Jiang, N., Liu, X.S. and Jiang, J.Q. (2017b) "Fracture analysis of double-layer hard and thick roof and the controlling effect on strata behavior: A case study", *Eng*. *Fail*. *Anal*., **81**, 117-134.

Ning, J.G., Wang, J., Tan, Y.L., Zhang, L.S. and Bu, T.T. (2017a), "In situ investigations into mining-induced overburden failures in close multiple-seam longwall mining: A case study", *Geomech*. *Eng*., **12**(4), 657-673.

Paul, P.S. (2016), "Rock mechanical investigation of strata loading characteristics to assess caving and requirement of support resistance in a mechanized powered support longwall face", *Int*. *J*. *Min*. *Technol*., **26(**6), 1081-1087.

Peng, S.S. (1987), "Support capacity and roof behaviour at longwall faces with shield supports", *Int*. *J*. *Min*. *Geol*. *Eng*., **5**(1), 29-57.

Peng, S.S. (2013), *Coal Mine Ground Control*, China University of Mining and Technology Press, Xuzhou, China.

Shen, B., King, A. and Guo, H. (2008), "Displacement, stress and seismicity in roadway roofs during mining-induced failure", *Int*. *J*. *Rock Mech*. *Min*. *Sci*., **45**(5), 672-688.

Singh, G.S.P. (2015), "Conventional approaches for assessment of caving behaviour and support requirement with regard to strata control experiences in longwall workings", *J*. *Rock Mech*. *Geotech*. *Eng*., **7**(3), 291-297.

Szwedzicki, T. (2001), "Geotechnical precursors to large-scale ground collapse in mines", *Int*. *J*. *Rock Mech*. *Min*. *Sci*., **38**(7), 957-965.

Tien, D.L., Oh, J., Hebblewhite, B., Zhang, C.G. and Mitra, R. (2018), "A discontinuum modelling approach for investigation of longwall top coal caving mechanisms", *Int*. *J*. *Rock Mech*. *Min*. *Sci*., **108**, 84-95.

Utsu, T., Ogata, Y. and Ritsuko, S. (1995), "The centenary of the omori formula for a decay law of aftershock activity", *J*. *Phys*. *Earth*, **43**(1), 1-33.

Wang, J., Ning, J., Jiang, L.S., Jiang, J.Q. and Bu, T.T. (2018), "Structural characteristics of strata overlying of a fully mechanized longwall face: A case study", *J*. *S*. *Afr*. *Inst*. *Min*. *Metall*., **118**(11), 1195-1204

Wang, J., Ning, J.G., Jiang, L.S., Gu, Q.H., Xu, Q.H. and Jiang, J.Q. (2017), "Effects of main roof fracturing on energy evolution during the extraction of thick coal seems in deep longwall faces", *Acta Geodyn*. *Geomater*., **14**(43), 377-387.

Yin, Y.C., Zhao, T.B., Zhang, Y.B., Tan, Y.L., Qiu, Y., Taheri, A. and Jing, Y. (2019), "An innovative method for placement of gangue backfilling material in steep underground coal mines", *Minerals*, **9**(2), 107.

Yin, Y.C., Zou, J.C., Zhang, Y.B., Qiu, Y., Fang, K. and Huang, D.M. (2018), "Experimental study of the movement of backfilling gangues for goaf in steeply inclined coal seams", *Arab*. *J*. *Geosci*., **11**(12), 318.

Zhang, C., Li, X.B., Dong, L.J., Ma J. and Huang, L.Q. (2016), "Analysis of microseismic activity parameters pre- and post roof caving and early warning", *Chin*. *J*. *Rock Mech*. *Eng*., **35**(s1), 3214-3221.

Zhang, G.C., Liang, S.J., Tan, Y.L., Xie, F.X., Chen, S.J. and Jia, H.G. (2018), "Numerical modeling for longwall pillar design, A case study from a typical longwall panel in China", *J*. *Geophys*. *Eng*., **15**(1), 121-134.

Zhang, P., Yang, T., Yu, Q., Xu, T., Zhu, W.C., Liu, H.L., Zhou, J.R. and Zhao, Y.C. (2015), "Microseismicity induced by fault activation during the fracture process of a crown pillar", *Rock Mech*. *Rock Eng*., **48**(4), 1673-1682.

JS